Oblate deformation in neutron-rich ^{118,119}Ag

E. H. Wang,[1] J. H. Hamilton,[1] A. V. Ramayya,[1] Y. X. Liu,[2] H. J. Li,[3] A. C. Dai,[4] W. Y. Liang,[4] F. R. Xu,[4] J. K. Hwang,[1] S. H. Liu,[1] N. T. Brewer,[1,*] Y. X. Luo,[1,5] J. O. Rasmussen,[5] Y. Sun,[6] S. J. Zhu,[3] G. M. Ter-Akopian,[7] and Yu. Ts. Oganessian[7]

[1]*Department of Physics and Astronomy, Vanderbilt University, Nashville, Tennessee 37235, USA*

[2]*Department of Physics, Huzhou University, Huzhou 313000, People's Republic of China*

[3]*Department of Physics, Tsinghua University, Beijing 100084, People's Republic of China*

[4]*Department of Physics, Peking University, Beijing 100871, People's Republic of China*

[5]*Lawrence Berkeley National Laboratory, Berkeley, California 94720, USA*

[6]*Department of Physics, Shanghai Jiao Tong University, Shanghai 200240, China*

[7]*Joint Institute for Nuclear Research, RU-141980 Dubna, Russian Federation*

(Received 3 February 2017; revised manuscript received 2 May 2017; published 14 June 2017)

High-spin-level schemes of ^{118,119}Ag are established for the first time by analyzing the high statistics γ-γ-γ and γ-γ-γ-γ coincidence data from the spontaneous fission of ^{252}Cf at Gammasphere. Two bands with 12 new levels in ^{118}Ag and three bands with 14 new levels in ^{119}Ag have been identified. A total Routhian surface calculation and projected shell model calculation have been performed to understand the behavior of these two nuclei. The calculations indicate oblate shape in ^{118,119}Ag.

DOI: 10.1103/PhysRevC.95.064311

I. INTRODUCTION

Neutron-rich Ag ($N = 47$) isotopes with three proton holes in the $Z = 50$ proton shell have drawn much attention since they lie in the transitional region. Previously, low-spin states of several Ag isotopes were reported in the β-decay work of Pd isotopes [1]. The $1/2^+[431]$ proton intruder orbital was reported to be the origin of the low-spin states [1]. The high-spin states of Ag nuclei in this region are usually associated with the $\pi g_{9/2}$ and $\nu h_{11/2}$ orbitals [2–5]. The interplay of these two orbitals can drive the nuclei into different shapes. Previously, global changes from $N = 50$ to $N = 82$ closed shell of odd-mass Ag nuclei have been compared [2,3]. Signature splittings from $N = 57$ to $N = 69$ even-mass Ag nuclei have been studied [5]. Phenomena of signature inversion [6], shape evolution [7], magnetic rotation [8], and chirality [9] have been reported in the $A \sim 110$ region. In the $A \sim 120$ region, our group studied the high-spin states of ^{115,117}Ag [10]. The $7/2^+[413]$ rotational bands were proposed. One band in ^{115}Ag [10] was reassigned to ^{116}Ag by Porquet *et al.* [5]. Porquet *et al.* reported the high-spin states of odd-odd ^{110,112,114,116}Ag [4,5].

Isomeric states were observed in β decay to ^{118,119}Ag [11–14] and isomeric- and ground-state β decay of ^{118}Ag [15] but no high-spin structures have been observed. In the present work, we have identified the coincidence γ rays and high-spin levels in ^{118,119}Ag by using their relation to the Sb ^{252}Cf spontaneous fission partners. The bands observed in the present work are related to the $7/2^+[413]$ proton orbital according our total Routhian surface (TRS) and projected shell model (PSM) calculations.

II. EXPERIMENTAL METHOD

The experiment with ^{252}Cf was carried out at the Lawrence Berkeley National Laboratory (LBNL). A 62-μ Ci ^{252}Cf source was sandwiched between two Fe foils of thickness 10 mg/cm^2 and was mounted in a 7.62-cm-diameter plastic (CH) ball to absorb β rays and conversion electrons. By using 101 Ge detectors of Gammasphere, high statistics of γ rays were detected with coincidences. The data were sorted into 5.7×10^{11} γ-γ-γ and higher fold γ events and 1.9×10^{11} γ-γ-γ-γ and higher fold γ coincident events. These γ coincident data were analyzed by the RADWARE software package [16]. More details of the experimental setups of these two experiments can be found in Refs. [17–19].

III. EXPERIMENTAL RESULTS

A. ^{118}Ag

The level scheme obtained in the current work is shown in Fig. 1. All the transitions are newly identified. Spins and parities are tentatively assigned according to the similarity to the neighboring ^{114,116}Ag nuclei [5]. Some of the β-decay work of ^{118}Pd and ^{118}Ag assigned $1^{(-)}$ for the ^{118}Ag ground state and $4^{(+)}$ for a 127.6-keV, 2.0-s isomer [13,15], while others proposed $(2)^-$ for the ground state and $(5)^+$ for the 127.6-keV isomer [12]. Thus, it is more probable that the whole level scheme decays to the 127.6-keV isomer or to some other isomer. The level scheme seems to form two band structures (yrast and yrare). The γ-ray transition intensities are listed in Table I. As seen in Table I, the $E2$ transition intensities out of the odd spin are much stronger than out of the even-spin ones, which may indicate an alternating $B(M1)/B(E2)$ branching ratio.

Figure 2(a) shows a γ coincidence spectrum in the low-energy region gated on the 162.3- and 168.1-keV transitions. The 277.8-, 320.8-, 388.3-, 549.7-, and 608.3-keV correlated transitions in ^{118}Ag can be seen. The low-energy fission partner

*Present address: Physics Division, Oak Ridge National Laboratory, Oak Ridge, TN 37831, USA.

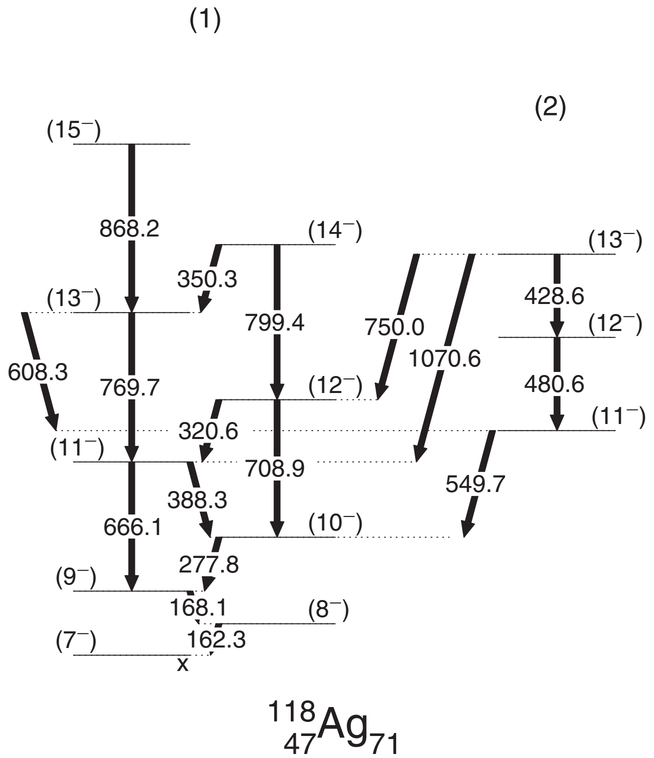

FIG. 1. Level scheme of ^{118}Ag obtained in the current work. All the transitions are newly identified.

transitions reported in ^{132}Sb [20] are also seen. Some of the strong contamination transitions labeled with the letter "c" in this spectrum come from ^{102}Nb and ^{147}La because of the 162.8-keV transition reported in ^{102}Nb [21], and the coincidence 167.7-keV transition decaying from the 167.7-keV level to the ground state in its fission partner ^{147}La. Figure 2(b) shows the high-energy region of the same gate. The 666.1-, 708.9-, 750.0-, 769.7-, 799.4-, 868.2-, and 1070.6-keV correlated transitions can be seen. The ^{129,130,131,133}Sb fission partner transitions previously reported [22–26] are also seen. The 895-keV transition in this spectrum is a contamination one from ^{154}Nd and caused by the 162.4-keV (4^+ to 2^+) transition in ^{154}Nd and the 167.0-keV transition ($3/2^+$ to $1/2^+$ g.s.) in its ^{252}Cf spontaneous fission (SF) partner ^{97}Sr. Figure 2(c) shows the low-energy region of γ ray spectrum gating on the 277.8- and 549.7-keV transitions. The 162.3-, 168.1-, 428.6-, 480.6-, and 608.3-keV transitions can be seen. Further analysis about mass assignment will be discussed later.

TABLE I. γ-ray energies, relative intensities, initial and final spin-parity assignments, and multipolarities of ^{118}Ag. Intensities are normalized to the 168.1-keV transition.

E_γ (keV)	I_γ	J_i^π	J_f^π	Multipolarity
162.3		(8^-)	(7^-)	$(M1/E2)$
168.1	100(6)	(9^-)	(8^-)	$(M1/E2)$
277.8	65(5)	(10^-)	(9^-)	$(M1/E2)$
320.6	15(1)	(12^-)	(11^-)	$(M1/E2)$
350.3	2.3(4)	(14^-)	(13^-)	$(M1/E2)$
388.3	29(2)	(11^-)	(10^-)	$(M1/E2)$
428.6	1.0(1)	(13^-)	(12^-)	$(M1/E2)$
480.6	3.3(3)	(12^-)	(11^-)	$(M1/E2)$
549.7	9.6(6)	(11^-)	(10^-)	$(M1/E2)$
608.3	2.1(2)	(13^-)	(11^-)	$(E2)$
666.1	21(1)	(11^-)	(9^-)	$(E2)$
708.9	6.1(5)	(12^-)	(10^-)	$(E2)$
750.0	4.4(3)	(13^-)	(12^-)	$(M1/E2)$
769.7	14(1)	(13^-)	(11^-)	$(E2)$
799.4	<2.5	(14^-)	(12^-)	$(E2)$
868.2	6.9(5)	(15^-)	(13^-)	$(E2)$
1070.6	5.0(4)	(13^-)	(11^-)	$(E2)$

B. ^{119}Ag

The level scheme of ^{119}Ag is shown in Fig. 3. All the transitions are newly identified except for the 130.0- and 507.2-keV transitions reported in ^{119}Pd β-decay work [14]. In Ref. [14], Penttila *et al.* reported isomers with tentative $1/2^-$ and $7/2^+$ spin and parity assignments. A 507.2-keV transition was also identified in Ref. [14] to be weakly in coincidence with the 130.0-keV transition. This 507.2-keV transition is proposed to decay from a $11/2^+$ level to a $9/2^+$ one within the current work. The 689.4-, 816.0-, and 860.3-keV $E2$ transitions are strong in the positive-parity bands in ^{119}Ag. The ^{117}Ag levels also show this phenomenon even after the sudden onset of shrinking $E2$ transition energy at $21/2^+$. Therefore, the 306.0- and 338.9-keV γ rays in ^{119}Ag are tentatively assigned as $E2$ transitions because $E2$ transitions are stronger than $M1$ in ^{117}Ag in this region. The relative intensities of the γ rays are listed in Table II. We note a writing mistake in the relative intensity of the 111.6 $M1$ transition of ^{117}Ag measured previously [10]. The listed value was 5.3 in Ref. [10] and it should be 0.5 according to the measurement in the current work. The $13/2^-$ and $19/2^-$ levels without bands built on them resemble the corresponding levels in band B reported in ^{115,117}Ag [10].

Figure 4(a) shows a γ-ray coincidence spectrum by double gating on 130.0 and 689.4 keV. In this spectrum, the 816.0-, 860.3-, 306.0-, and 338.9-keV transitions in band 1, the 731.0-keV transition, and all the transitions in bands 2 and 3 can be seen. The intensities of the transitions in bands 2 and 3 give their order in the high-spin negative parity band. The presence of ^{129,130,131}Sb transitions and the absence of ^{133}Sb transitions in this spectrum confirm the current mass assignment of ^{119}Ag. Figure 4(b) shows a γ-ray coincidence spectrum gated on the 130.0- and 507.2-keV transitions. In this spectrum, the 182.2-, 306.0-, 338.9-, 816.0-, and 860.3-keV transitions in the positive-parity band; the 159.3-, 189.0-, 221.1-, 254.2-, 263.1-, and 319.2-keV transitions in the negative-parity band; and the 536.4-, 559.7-, and 913.9-keV interband transitions can be seen. The 331- and 431-keV peaks are contamination transitions from ^{144}Ba, which are fed by a 509-keV transition and depopulated by 130-keV Comptons of the 199-keV 2-0 transition. The 1221.6-keV peak is a contamination 2-0 transition from ^{130}Sn which is in coincidence with the 129.8-keV transition in ^{130}Sn and the 505.9-keV 2-0 transition in its fission partner ^{120}Cd. Our data

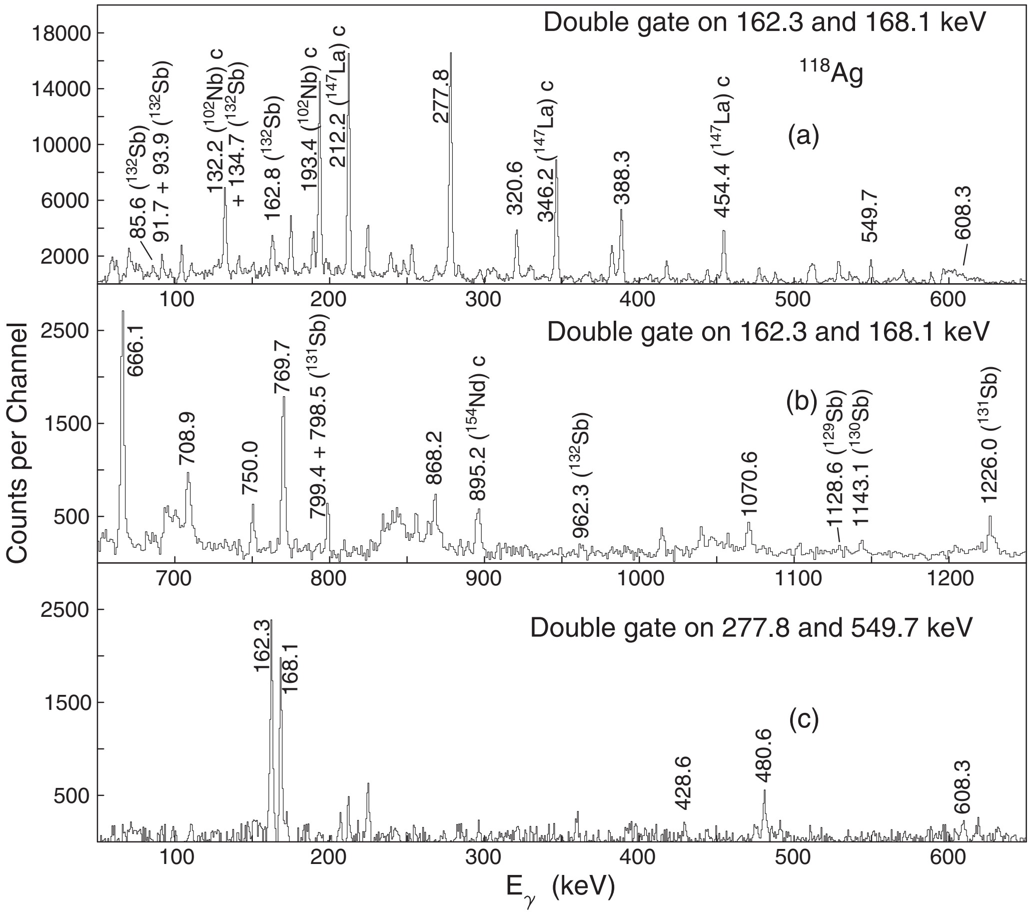

FIG. 2. Partial γ coincidence spectra by (a) double gating on 162.3- and 168.1-keV transition to show the low-energy region, (b) double gating on 162.3- and 168.1-keV transition to show the high-energy region, and (c) double gating on 277.8- and 549.7-keV transition to show a low-energy region. The "c" identifies known contaminant lines.

also show weak evidence for 136.4- and 285.6-keV transitions feeding the $25/2^+$ level. They are not placed in the level scheme. Further analysis about mass assignments will be discussed later.

C. Mass determination

Figure 5 shows the γ-ray coincidence spectra gating on transitions in $^{115-119}$Ag from Figs. 5(a) to 5(e). Only high-energy $^{129-131,133}$Sb fission partner transitions are labeled in the spectra. Note that the 118.3- to 311.2-keV cascade was assigned to ^{115}Ag in ^{252}Cf SF [10] and then assigned to ^{116}Ag in ^{18}O + ^{208}Pb fusion fission work [5]. The relative intensities of the 1510.1- and 2791.3-keV transitions in ^{133}Sb decrease as A increases from 115 to 118. The ^{133}Sb transitions are very weak in the ^{118}Ag transitions gate. In contrast, the intensity of the ^{131}Sb transition increases as A increases from 115 to 118. The intensity of the 1128.6-keV transition in ^{129}Sb is much smaller than the 1226.0-keV one in ^{131}Sb in the ^{118}Ag gate in Fig. 5(d). In the ^{119}Ag transition gate in Fig. 5(e), these two transitions in ^{129,131}Sb are almost equal. Also, the relative intensity of the 1143-keV transition in ^{130}Sb increases as A increases from 117 to 119. Thus, these spectra give evidence for the mass

TABLE II. γ-ray energies, relative intensities, and initial and final spin-parity assignments and multipolarities of ^{119}Ag. Intensities are normalized to the 689.4-keV transition.

E_γ (keV)	I_γ	J_i^π	J_f^π	Multipolarity
130.0		$(9/2^+)$	$(7/2^+)$	$(M1/E2)$
159.3	14(1)	$(21/2^-)$	$(19/2^-)$	$(M1/E2)$
182.2	32(2)	$(13/2^+)$	$(11/2^+)$	$(M1/E2)$
189.0	32(2)	$(15/2^-)$	$(13/2^-)$	$(M1/E2)$
221.1	31(2)	$(17/2^-)$	$(15/2^-)$	$(M1/E2)$
254.2	6.1(5)	$(21/2^-)$	$(19/2^-)$	$(M1/E2)$
263.1	10(1)	$(23/2^-)$	$(21/2^-)$	$(M1/E2)$
306.0	17(1)	$(23/2^+)$	$(21/2^+)$	$(M1/E2)$
319.2	6.0(5)	$(25/2^-)$	$(23/2^-)$	$(M1/E2)$
338.9	16(1)	$(25/2^+)$	$(23/2^+)$	$(M1/E2)$
507.2	41(5)	$(11/2^+)$	$(9/2^+)$	$(M1/E2)$
536.4	20(1)	$(13/2^-)$	$(11/2^+)$	$(E1)$
559.7	9.5(7)	$(15/2^-)$	$(13/2^-)$	$(M1/E2)$
689.4	100(7)	$(13/2^+)$	$(9/2^+)$	$(E2)$
731.0	9.4(7)	$(19/2^-)$	$(17/2^+)$	$(E1)$
816.0	48(4)	$(17/2^+)$	$(13/2^+)$	$(E2)$
860.3	20(2)	$(21/2^+)$	$(17/2^+)$	$(E2)$
913.9	26(2)	$(15/2^-)$	$(13/2^+)$	$(E1)$

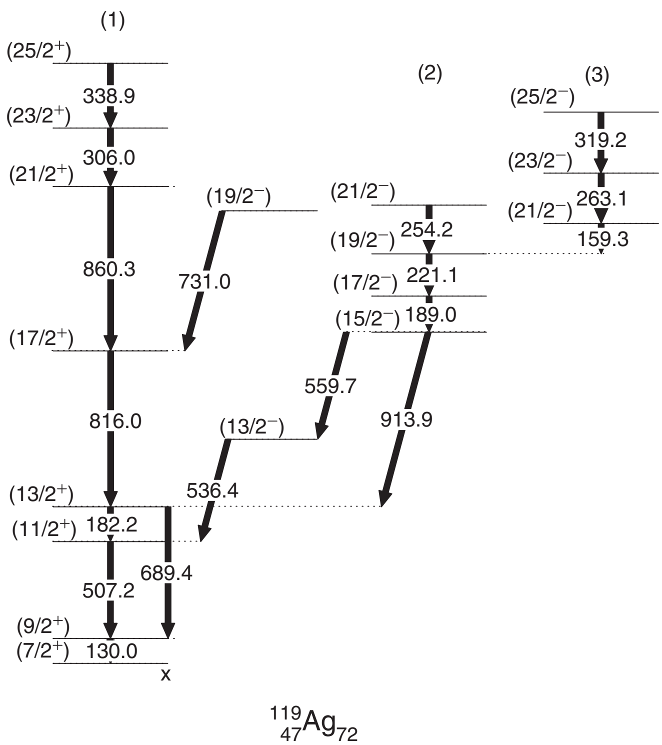

FIG. 3. Level scheme of ^{119}Ag obtained in the current work. The 130- and 507-keV transitions were reported in β-decay work previously [14]. Other transitions are newly identified.

assignments of ^{115,117}Ag in Ref. [10], ^{116}Ag in Ref. [5], and ^{118,119}Ag in the current work. Hwang *et al.* also reported a 223.8- to 178.3-keV cascade in ^{114}Ag [10]. In the present work, these two transitions are assigned to ^{133}Sb and proposed to feed the 4301.7-keV level. We note that the previously reported [27] high-energy transitions populating the (8^-) 4.2-min isomer in ^{132}Sb are not very clearly seen in the ^{118}Ag gate. However, those transitions can be clearly seen in the $^{115-117}$Ag gates in our data. Such phenomenon may be due to the odd-even effect.

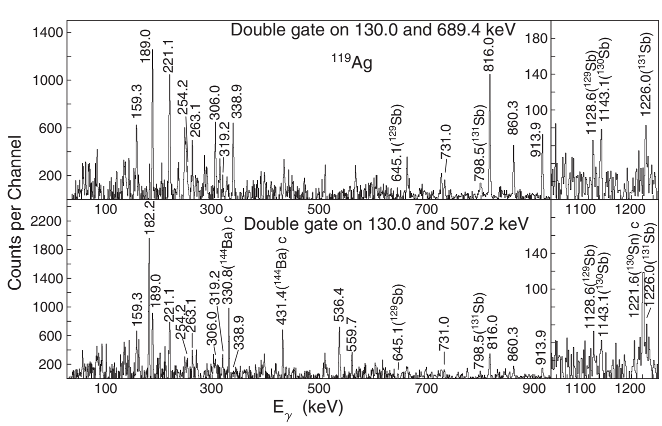

FIG. 4. Partial γ coincidence spectra by (a) double gating on 130.0 and 689.4 keV and (b) double gating on 130.0 and 507.2 keV. The "c" identifies known contaminant lines.

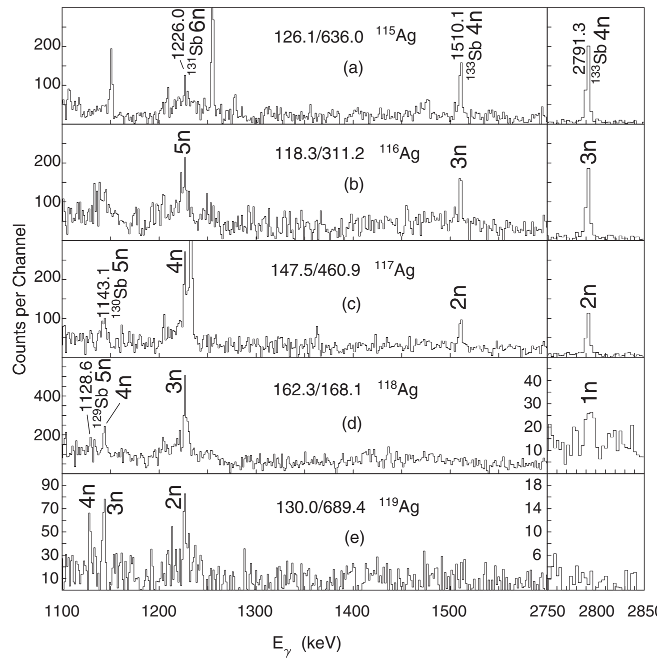

FIG. 5. Partial γ-coincidence spectra by gating on transitions from $^{115-119}$Ag. Transitions are taken from Refs. [5,10] and the current work. The ^{129,130,131,133}Sb fission partner transitions are indicated with neutron evaporation numbers. Note that the count scale of the high-energy regions of parts (d) and (e) have been changed.

IV. DISCUSSION

A. ^{118}Ag

Odd-odd Ag nuclei in this region with a $Z = 47$ proton number are close to the $Z = 50$ closed shell. Low excited states of these nuclei usually have small deformation and show single-particle properties. The levels of ^{118}Ag are similar to the yrast negative-parity bands in neighboring odd-odd Ag isotopes as shown in Fig. 6. The energy spacing of these odd-odd Ag nuclei are irregular from 6^- to 9^- states, while above the 9^- state, they exhibit common rotational band patterns. The energyspacing shows gradual increasing from ^{104}Ag to ^{108}Ag, decreasing from ^{108}Ag to ^{116}Ag and nearly the same in ^{116}Ag to ^{118}Ag. The smooth change supports the current spin and parity assignments. These bands in Ag isotopes were assigned to a $g_{9/2} \otimes h_{11/2}$ or $g_{9/2}^{-1} \otimes h_{11/2}$ configuration [4,5,28–32]. The band (1) in ^{118}Ag is proposed to have the same configuration in the current work. The shrinking $E(8^-)$-$E(6^-)$ energy spacings in ^{104,106,108}Ag were the bases for proposed two unobserved low-energy transitions from the 8^- to 7^- levels and from the 7^- to 6^- levels in ^{114,116}Ag [5]. So, in ^{118}Ag the 7^- to 6^- transition may be too low in energy to be seen. The interpretations of these bands in the $A < 110$ region have been controversial. Datta *et al.* gave a soft triaxial shape for ^{104}Ag [28]. Joshi *et al.* suggested a soft triaxial shape for the band in ^{106}Ag [29], while Lieder *et al.* proposed an axially deformed shape ($\beta_2 = 0.22, \gamma = 0^\circ$) [30]. Similarly, ^{108}Ag was assigned to have an axially deformed shape ($\beta_2 = 0.16, \gamma = 0^\circ$) by Liu *et al.* [31]. Roy *et al.* suggested a triaxial shape ($\gamma = 20^\circ$) for ^{110}Ag [32]. The phenomena of shape evolution, signature

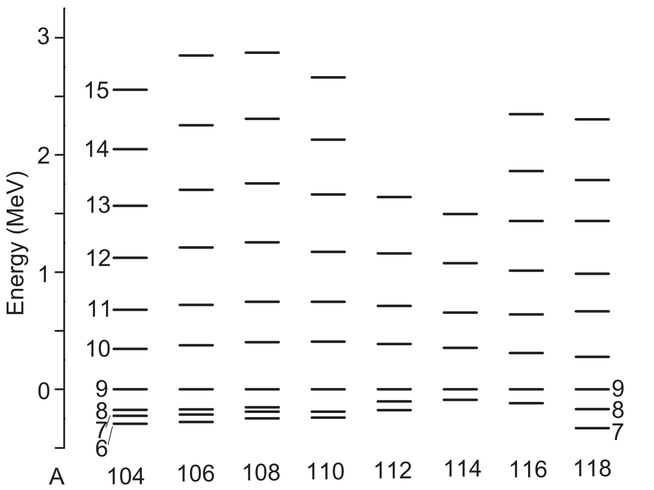

FIG. 6. Comparison of energy levels (up to 15^-) of yrast negative-parity bands in even-A Ag isotopes of $^{104-118}$Ag. Level energies are normalized to zero for the 9^- levels. Data are taken from Refs. [4,5,28–32] and the current work.

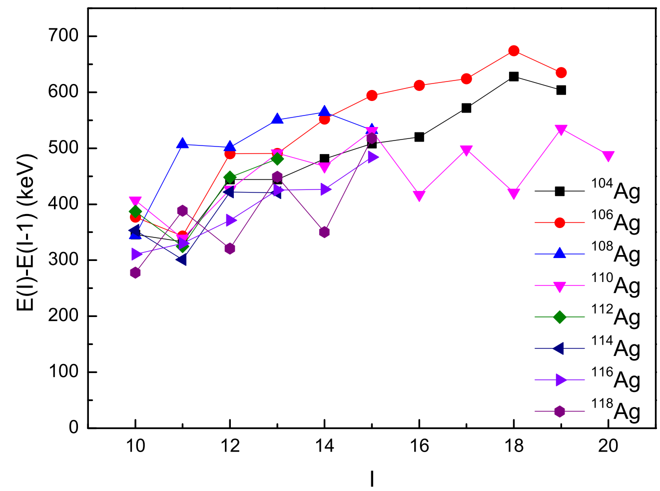

FIG. 7. Comparison of $E(I) - E(I-1)$ vs I of the negative-parity bands in even-A Ag isotopes of $^{104-118}$Ag.

inversion, magnetic rotation, and chiral doublet bands have been reported in the region of $A < 110$ based on different deformations [28–31].

Signature inversion studies of the negative-parity $g_{9/2} \otimes h_{11/2}$ bands in odd-odd Ag nuclei have been an important issue [33]. The ^{118}Ag nucleus is the most neutron-rich one with such a band observed in the Ag isotopic chain. The inversion spins for the odd-odd Ag isotopic chains have been systematically compared [33]. As reported in Ref. [33], all the favored signature branch lies higher in energy at relatively lower spin than the unfavored branch. The reported inversion points [33] shift from $I = 15$ for ^{104,106,108}Ag, $I = 14$ for ^{110}Ag, to $I = 13$ for ^{116}Ag. Such phenomenon was interpreted as the competition between Coriolis force and the proton-neutron interactions. In the current work, the inversion point is about $I = 9$ for ^{118}Ag. The dramatic change of inversion point in ^{118}Ag needs further theoretical discussion. After the inversion point, these nuclei show different behavior. Figure 7 shows the $E(I) - E(I-1)$ curves in $^{104-118}$Ag nuclei. Pronounced staggering can be seen in ^{110}Ag and ^{118}Ag while the other curves are relatively smooth. Also, signature inversion occurs in ^{116}Ag. The large staggering in ^{118}Ag could be related to a change of γ values or the evolution from tilted axis rotation (TAR) to principal axis rotation (PAR). Note that PAR was presented in ^{110}Ag [32] and ^{114}Rh [34]. However, similar staggering of the $B(M1)/B(E2)$ branching ratio has been observed in ^{118}Ag in the current work.

We carried out total Routhian surface calculations for odd-odd Ag nulei shown in Fig. 8. The result indicates oblate shape ($\gamma \approx -65^\circ$ to -60°) for ^{118}Ag at frequencies above $\hbar\omega = 0.1$ MeV. The calculation predicts a backbending at $\hbar\omega = 0.4$–0.5MeV, which cannot be observed at the frequency in the current work. Our calculation also show $\beta_2 \approx 0.22$, $\gamma \approx -65^\circ$ for ^{114,116}Ag. These values are consistent with the triaxial oblate in ^{112}Pd ($N = 66$), nearly oblate in ^{114,116}Pd ($N = 68$, 70), and then back to triaxial oblate in ^{118}Pd ($N = 72$) reported from TRS calculations [35].

A projected shell model (PSM) calculation has been carried out for the transition energies in ^{118}Ag as shown in Fig. 9. The calculation used $\epsilon_2 = -0.210$, $\epsilon_4 = 0.063$ oblate parameters. The ground state of ^{118}Ag was calculated to be $1^-\ \pi 1/2[301]+\nu 3/2[402]$ and the bandhead of the current

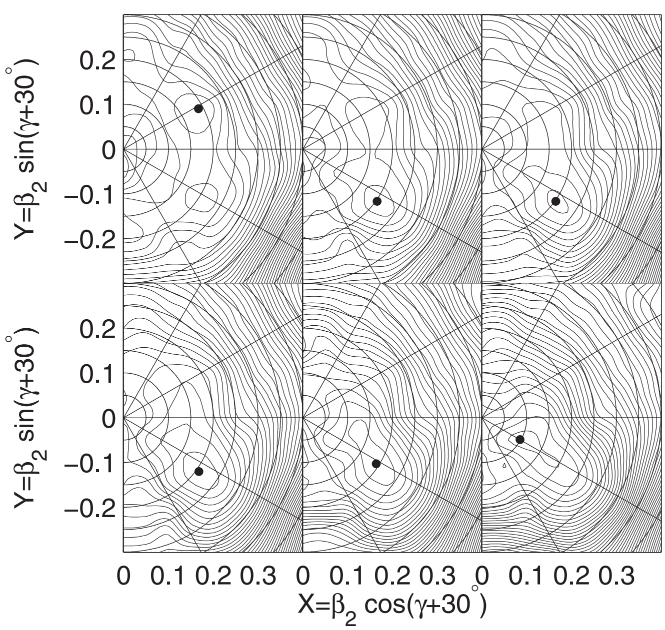

FIG. 8. Calculated total Routhian surface of proton positive-parity signature and neutron negative-parity positive signature for ^{118}Ag. The contour lines are 300-keV increments. The corresponding rotational frequency and minimums are, top left to right and bottom left to right, $\hbar\omega = 0.0$ MeV, $\beta_2 = 0.190$, $\gamma = -2^\circ$, $\hbar\omega = 0.1$ MeV, $\beta_2 = 0.203$, $\gamma = -65^\circ$; $\hbar\omega = 0.2$ MeV, $\beta_2 = 0.203$, $\gamma = -65^\circ$; $\hbar\omega = 0.3$ MeV, $\beta_2 = 0.206$, $\gamma = -65^\circ$; $\hbar\omega = 0.4$ MeV, $\beta_2 = 0.193$, $\gamma = -62^\circ$; $\hbar\omega = 0.5$ MeV, $\beta_2 = 0.098$, $\gamma = -60^\circ$. Note in polar coordinate β_2 is always positive and γ indicates the prolate and oblate shapes.

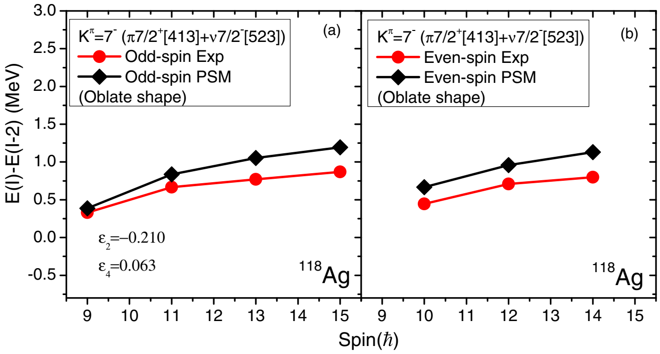

FIG. 9. Projected shell model calculation of the 7^- band in ^{118}Ag, compared with experimental data.

levels was suggested to be 7^- $\pi7/2[413]+\nu7/2[523]$ isomer. The conclusion is consistent with the shape trends in the neighboring Pd isotopes. Note that shape evolution at low spins from triaxial prolate in ^{110}Pd ($N = 64$) via triaxial oblate in ^{112}Pd ($N = 66$) to nearly oblate in ^{114,116}Pd ($N = 68, 70$), and then back to triaxial oblate in ^{118}Pd ($N = 72$) was reported from TRS calculations [36,37]. The finite-range liquid drop model also predicted oblate shapes in $^{112–119}$Ag [38]. The trend of the $E2$ transition energies was well reproduced by the PSM calculation. The calculation assumed the 106.3-keV (theoretical result) transition decays from a 8^- state to a 7^- state. As discussed above, the transition energy from 8^- to 7^- is very low energy in ^{104,106,108}Ag.

In the PSM calculation, we take the deformed basis as a good start by using the deformed Nilsson single-particle states at fixed oblate deformations in all spin region for ^{118}Ag. It can be seen from Fig. 8 that the shape coexistences dominate the behavior of low-spin region. Mixing of different shapes can drive the system away from an ideal rotor behavior. Our PSM theory, however, assumes a fixed deformation in the model basis.

B. ^{119}Ag

The energy levels in ^{119}Ag are similar to those in ^{115,117}Ag below the $21/2^+$ state (Fig. 10). The positive-parity bands in ^{115,117}Ag were assigned as $7/2^+[413]$ based on prolate shape [10]. On the oblate side from our TRS calculation (Fig. 11), such configuration is unlikely rather than a low Ω orbital of the $g_{9/2}$ shell. This band could have a $g_{9/2}$ configuration if ^{119}Ag has a near spherical shape. Above the $21/2^+$ state of ^{119}Ag, the 306- and 339-keV transitions in ^{119}Ag could be $M1$ or $E2$. But back bending occurs here in either way for ^{119}Ag as well as ^{117}Ag. The first back bending of the even-even Pd core in this region originates from the alignment of a pair of $g_{9/2}$ protons or a pair of $h_{11/2}$ neutrons from TRS [35] and projected shell model (PSM) calculations [39]. Thus, the alignment of $h_{11/2}$ neutrons can give rise to the back bending in ^{117,119}Ag because the alignment of a pair of protons should be blocked. Back bending in ^{115}Ag was not observed according to the levels reported in Ref. [10]. The two signatures of band 1 in ^{119}Ag have similar energy levels. Signature splittings for these positive-parity bands in ^{115,117,119}Ag are also similar.

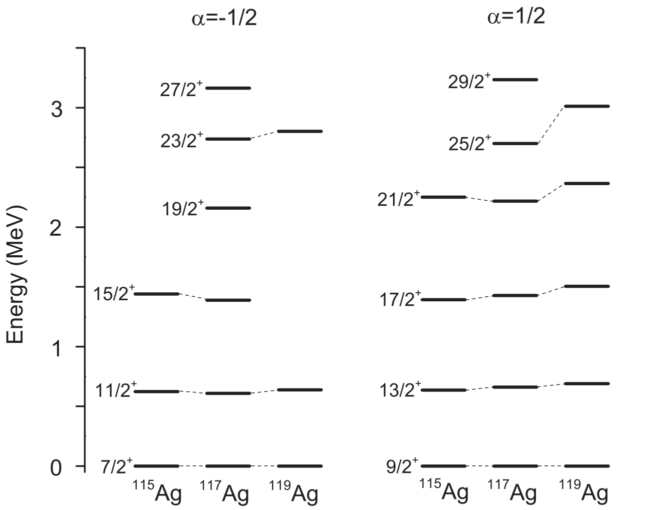

FIG. 10. Comparison of energy spacing of the $7/2^+$ bands in $^{115–119}$Ag. Level energies are normalized to the $7/2^+$ and $9/2^+$ states, respectively.

Previously, the bands in ^{115,117}Ag built on the $7/2^+$ state were proposed as a consequence of γ softness or triaxiality [10]. A similar explanation for ^{119}Ag can be confirmed from the TRS calculations in Fig. 11. However, the calculations show a more complicated behavior of this nucleus at different rotational frequency. The signature splitting in ^{115,117}Ag were interpreted as K mixing caused by triaxiality in the Ag isotopes in Ref. [40] and as the evolution of a $\pi g_{9/2}^{-3}$ cluster in Refs. [2,3].

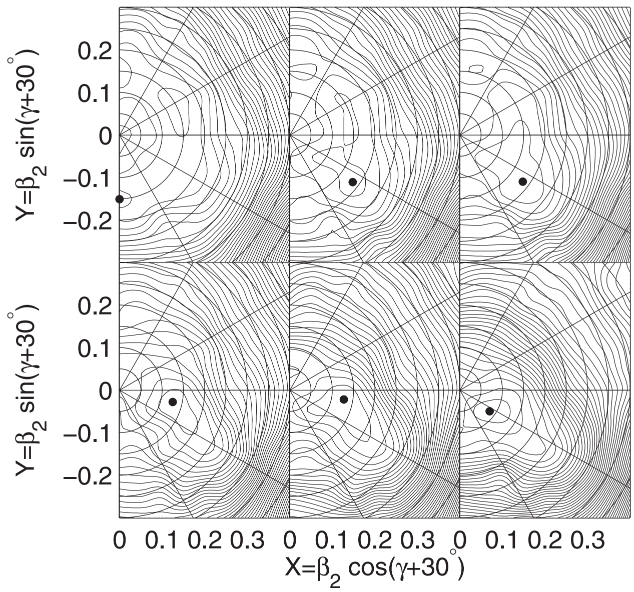

FIG. 11. Calculated total Routhian surface of proton positive-parity positive signature for ^{119}Ag. The contour lines are 300-keV increments. The corresponding rotational frequency and minimums are $\hbar\omega = 0.0$ MeV, $\beta_2 = 0.151$, $\gamma = -120°$; $\hbar\omega = 0.1$ MeV, $\beta_2 = 0.185$, $\gamma = -67°$; $\hbar\omega = 0.2$ MeV, $\beta_2 = 0.184$, $\gamma = -67°$; $\hbar\omega = 0.3$ MeV, $\beta_2 = 0.129$, $\gamma = -43°$; $\hbar\omega = 0.4$ MeV, $\beta_2 = 0.129$, $\gamma = -40°$; $\hbar\omega = 0.5$ MeV, $\beta_2 = 0.086$, $\gamma = -65°$.

TABLE III. Excited quasiparticle states of ^{119}Ag from PES calculation. Configurations, shape parameters, and excitation energies are indicated in the table.

Configuration	β_2	γ (deg)	β_4	E_{exc} (keV)
$\pi 7/2^+[413]$	0.121	0	−0.006	0
$\pi 1/2^-[301]$	0.153	−41	−0.026	8
$\pi 1/2^+[440]$	0.096	−59	−0.015	25
$\nu 7/2^-[523] \otimes 1/2^+[400] \otimes \pi 7/2^+[413]$	0.144	−42	−0.021	1786
$\nu 5/2^-[532] \otimes 3/2^+[402] \otimes \pi 7/2^+[413]$	0.102	0	−0.008	1911

Here we have also undertaken PES calculations to provide the contour maps of potential energies for the low-lying states in ^{119}Ag with results in Table III. In such PES calculations, the total energy of a nucleus are decomposed into macroscopic and microscopic parts. For the macroscopic part, the standard liquid-drop model [41] is employed. Meanwhile, the deformed Woods-Saxon (WS) model [42] is used to calculate the the microscopic part. To reduce the unphysical fluctuation of the weakened pairing field (from the unpaired nucleons), an approximate particle-number projection, known as the Lipkin-Nogami method [43], is employed. In the configuration-constrained PES calculation, it is required to adiabatically block the unpaired nucleon orbits that specify the given configuration. This approach is achieved by calculating and identifying the average Nilsson quantum numbers for every evolved orbit in a configuration [44]. In the calculations, the equilibrium deformation is determined by minimizing the obtained PES in the lattice of quadrupole (β_2, γ) deformations with hexadecapole (β_4) variation.

The PES calculations assign the ground state as $7/2^+[413]$ with a prolate shape. Meanwhile, the calculated $1/2^-[301]$ and $1/2^+[440]$ states are very low lying in energies with oblate shapes. The calculation also provide possible assignments of the configurations of band 2. The bandhead of band 2 is 1733 keV higher than the $7/2^+$ state in experiment. Thus, the best guess would be $\nu 7/2^-[523] \otimes \nu 1/2^+[400] \otimes \pi 7/2^+[413]$ with oblate shape.

PSM calculation has been carried out for the transition energies in ^{119}Ag as shown in Fig. 12. The calculations used $\epsilon_2 = -0.215$, $\epsilon_4 = 0.033$ parameters. The calculations also predict the ground state of ^{119}Ag will have a $1/2^-[301]$ orbital and the new positive band will have a $\pi 7/2^+[413]$ orbital. According to the calculations, the back bending can be reproduced for oblate parameters but not for prolate parameters. This calculation shows evidence for an oblate shape in ^{119}Ag.

To understand the variation of $E(I) - E(I-2)$ with spin in Fig. 12, we plot a band diagram in Fig. 13. There are typically six 1-quasiparticle (qp) bands and three 3-qp bands, each of which has a K given by the sum of the Nilsson K quantum numbers of its constituent quasiparticles. Superposition of them imposed by configuration mixing gives the final results, with dots in Fig. 13 representing the lowest state at each angular momentum. The important configurations of 1-qp and 3-qp

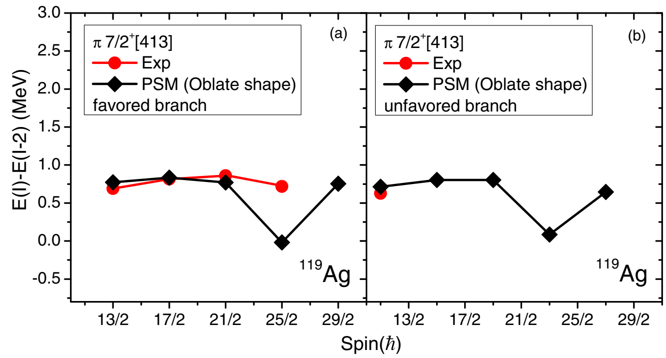

FIG. 12. Projected shell model calculation of the $7/2^+$ band in ^{119}Ag, compared with experimental data.

bands shown in Fig. 13 are listed in Table IV. An interesting observation in Fig. 13 is the irregular structures in some bands, such as those in the $\pi 1/2[440]$. In a plot of energy versus spin, a staggering or zigzag pattern can be seen. These irregularities are attributed to the decoupling effect [45], which is usually seen in rotational bands with a high-j and low-K state (e.g., $K = 1/2$ or $K = 3/2$) as the main configuration. For the $K = 1/2$ and $K = 3/2$ bands, a pronounced zigzag pattern is seen for almost the entire spin range.

In Fig. 12, calculated $E(I) - E(I-2)$ as functions of spin and comparison with the present data are plotted for $\pi 7/2[413]$ 1-qp band of ^{119}Ag. The calculation and comparison suggest that the $E(I) - E(I-2)$ almost keeps constant at low spins. It, however, shows a decreasing trend at high spins, and a dip is present at spins $I = 21/2$–$25/2$. To understand these

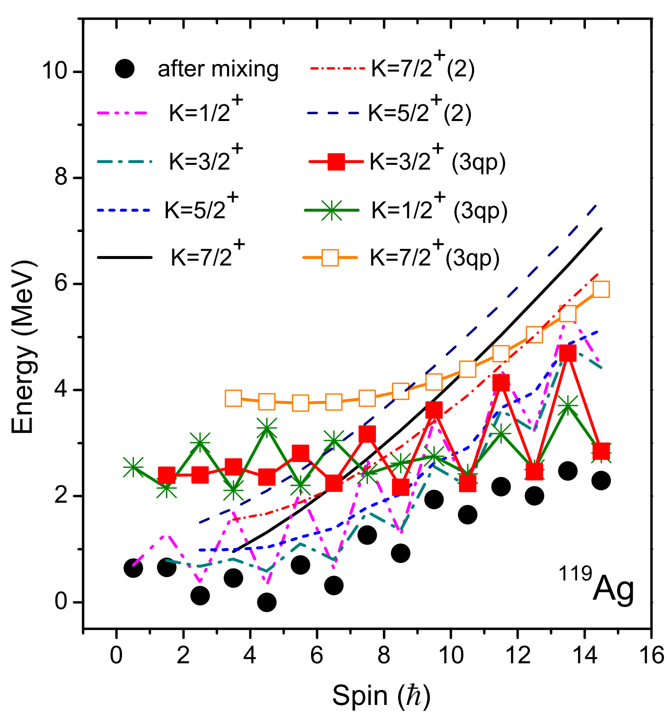

FIG. 13. Band diagram. The 1-qp bands and 3-qp bands are plotted for ^{119}Ag.

TABLE IV. Important configurations of positive-parity 1- and 3-qp bands for ^{119}Ag.

qp	Total K	Configuration
1-qp	1/2	$\pi 1/2[440]$
	3/2	$\pi 3/2[431]$
	5/2	$\pi 5/2[422]$
	7/2	$\pi 7/2[413]$
	5/2(2)	$\pi 5/2[413]$
	7/2(2)	$\pi 7/2[404]$
3-qp	3/2	$\pi 1/2[440]\oplus\nu 5/2[532]\oplus\nu 3/2[541]$
	1/2	$\pi 1/2[440]\oplus\nu 5/2[532]\oplus\nu 3/2[541]$
	7/2	$\pi 5/2[413]\oplus\nu 5/2[532]\oplus\nu 7/2[532]$

variations in $E(I) - E(I-2)$, we recall the band diagram in Fig. 13. Two 3-qp bands with $K = 1/2$ and $K = 3/2$ cross with $\pi 7/2[413]$ at spin $I = 13/2$–$17/2$; however, the phase of zigzag pattern is opposite, and the $E(I) - E(I-2)$ is influenced little and almost keeps constant with spin in Fig. 12. Due to the second crossing of $K = 7/2$ 3-qp band with $\pi 7/2[413]$ 1-qp band at spins $I = 21/2$–$25/2$, the $E(I) - E(I-2)$ values decrease and a dip is present. Thus, these crossings modify the structure of rotational bands, which is reflected in the variations of energy.

It is worth noting that the ^{119}Ag is a very soft nucleus with small deformation without cranking. Theoretical approaches on such kinds of nucleus would make it difficult to give a full explanation. Both PES and PSM calculations predict small deviations between the $7/2^+$ and $1/2^-$ states. Furthermore, oblate shapes are also given by the low-lying $1/2^-$ and $1/2^+$ states in PES calculations. Thus, the different assignments of the ground state between these two calculations are not seriously contradictive. The shape provided in PES calculations would become hard oblate with increasing rotational frequency. In all, the ^{119}Ag is generally an oblate nucleus but prolate and oblate shape coexistence is also possible, as shown in systematic calculations in this region [36].

The negative-parity band in ^{119}Ag with $15/2^-$ bandhead is similar to the negative "bands C" reported in ^{115,117}Ag [10]. These bands could be magnetic rotation bands or 1 proton + 2 neutron three-quasiparticle bands because of the strong $M1$ transitions and the unobserved $E2$ transitions. The bands 2 and 3 need further theoretical consideration.

V. CONCLUSION

The present work establishes high spin level schemes of ^{118,119}Ag nuclei for the first time by analyzing the γ ray coincidences from ^{252}Cf with Gammasphere. The level schemes of these two nuclei show similarity to the lighter odd-odd and odd-even Ag nuclei, respectively. We propose band 1 of ^{118}Ag to be $\pi g_{9/2} \otimes \nu h_{11/2}$ and the band 1 of ^{119}Ag to be $\pi g_{9/2}$. The TRS calculation was used to interpret the shape of these two nuclei.

ACKNOWLEDGMENTS

The work at Vanderbilt University and Lawrence Berkeley National Laboratory is supported by the U.S. Department of Energy under Grant No. DE-FG02-88ER40407 and Contract No. DE-AC03-76SF00098. The work at Tsinghua University was supported by the National Natural Science Foundation of China under Grant No. 11175095. The work at JINR was partially supported by the Russian Foundation for Basic Research Grant No. 08-02-00089 and by the INTAS Grant No. 03-51-4496. The work at SJTU in Shanghai was supported by the National natural science foundation of China under Grant No. 11575112, by the 973 Program of China (Grant No. 2016YFA0400501 and No. 2013CB834401). The work at HUTC in Huzhou was supported by the NNSF of China Grants No. 11647306 and No. 11475062. The authors give special thank to Q.B. Chen in Peking University and the theoretical group for private communications.

[1] J. Rogowski, J. Alstad, S. Brant, W. R. Daniels, D. DeFrenne, K. Heyde, E. Jacobs, N. Kaffrell, V. Paar, G. Skarnemark *et al.*, Phys. Rev. C **42**, 2733 (1990).

[2] S. Lalkovski, A. M. Bruce, A. Jungclaus, M. Górska, M. Pfützner, L. Cáceres, F. Naqvi, S. Pietri, Zs. Podolyák, and G. S. Simpson *et al.*, Phys. Rev. C **87**, 034308 (2013).

[3] I. Stefanescu, W. B. Walters, P. F. Mantica, B. A. Brown, A. D. Davies, A. Estrade, P. T. Hosmer, N. Hoteling, S. N. Liddick, and W. D. M. Rae, Eur. Phys. J. A **42**, 407 (2009).

[4] M.-G. Porquet, Ts. Venkova, P. Petkov, A. Bauchet, I. Deloncle, A. Astier, N. Buforn, J. Duprat, B. J. P. Gall, C. Gautherin *et al.*, Eur. Phys. J. A **15**, 463 (2002).

[5] M.-G. Porquet, Ts. Venkova, A. Astier, A. Bauchet, I. Deloncle, N. Buforn, L. Donadille, O. Dorvaux, B. J. P. Gall, and S. Lalkovski *et al.*, Eur. Phys. J. A **18**, 25 (2003).

[6] J. Timár, J. Gizonb, A. Gizonb, D. Sohler, B. M. Nyakó, L. Zolnai, D. Bucuresu, Gh. Căta-Danil, A. J. Boston, D. T. Joss *et al.*, Acta Phys. Pol. B **33**, 493 (2002).

[7] K. Heyde and J. L. Wood, Rev. Mod. Phys. **83**, 1467 (2011).

[8] H. Hübel, Prog. Part. Nucl. Phys. **54**, 1 (2005).

[9] S. Frauendorf and J. Meng, Nucl. Phys. A **617**, 131 (1997).

[10] J. K. Hwang, A. V. Ramayya, J. H. Hamilton, C. J. Beyer, X. Q. Zhang, J. O. Rasmussen, Y. X. Luo, S. C. Wu, T. N. Ginter, I. Y. Lee *et al.*, Phys. Rev. C **65**, 054314 (2002).

[11] V. Koponen, J. Äystö, J. Honkanen, P. Jauho, H. Penttilä, J. Suhonen, P. Taskinen, K. Rykaczewski, J. Żylicz, and C. N. Davids, Z. Phys. A **333**, 339 (1989).

[12] Z. Janas, J. Äystö, K. Eskola, P. P. Jauho, A. Jokinen, J. Kownacki, M. Leino, J. M. Parmonen, H. Penttillä, J. Szerypo *et al.*, Nucl. Phys. A **552**, 340 (1993).

[13] J. Hill, IS-4351, Iowa State University Research Report, Ames, 1979 (unpublished).

[14] H. Penttila, J. Äystö, K. Eskola, Z. Janas, P. P. Jauho, A. Jokinen, M. E. Leino, J. M. Parmonen, and P. Taskinen, Z. Phys. A **338**, 291 (1991).

[15] B. Fogelberg, A. Bäcklin, and T. Nagarajan, Phys. Lett. B **36**, 334 (1971).
[16] D. C. Radford, Nucl. Instrum. Methods Phys. Res., Sect. A **361**, 297 (1995).
[17] J. H. Hamilton, A. V. Ramayya, S. J. WU, G. M. Ter-Akopian, Yu. Ts. Oganessian, J. D. Cole, J. O. Rasmussen, and M. A. Stoyer, Prog. Part. Nucl. Phys. **35**, 635 (1995).
[18] J. K. Hwang, A. V. Ramayya, J. H. Hamilton, D. Fong, C. J. Beyer, P. M. Gore, Y. X. Luo, J. O. Rasmussen, S. C. Wu, I. Y. Lee *et al.*, Phys. Rev. C **67**, 054304 (2003).
[19] E. H. Wang, A. Lemasson, J. H. Hamilton, A. V. Ramayya, J. K. Hwang, J. M. Eldridge, A. Navin, M. Rejmund, S. Bhattacharyya, S. H. Liu *et al.*, Phys. Rev. C **92**, 034317 (2015).
[20] C. A. Stone, S. H. Faller, and W. B. Walters, Phys. Rev. C **39**, 1963 (1989).
[21] J. K. Hwang, A. V. Ramayya, J. Gilat, J. H. Hamilton, L. K. Peker, J. O. Rasmussen, J. Kormicki, T. N. Ginter, B. R. S. Babu, C. J. Beyer *et al.*, Phys. Rev. C **58**, 3252 (1998).
[22] J. Genevey, J. A. Pinston, H. R. Faust, R. Orlandi, A. Scherillo, G. S. Simpson, I. S. Tsekhanovich, A. Covello, A. Gargano, and W. Urban, Phys. Rev. C **67**, 054312 (2003).
[23] J. Genevey, J. A. Pinston, C. Foin, M. Rejmund, H. Faust, and B. Weiss, Phys. Rev. C **65**, 034322 (2002).
[24] J. Genevey, J. A. Pinston, H. Faust, C. Foin, S. Oberstedt, and M. Rejmund, Eur. Phys. J. A **9**, 191 (2000).
[25] W. Urban, W. Kurcewicz, A. Korgul, P. J. Daly, P. Bhattacharyya, C. T. Zhang, J. L. Durell, M. J. Leddy, M. A. Jones, W. R. Phillips *et al.*, Phys. Rev. C **62**, 027301 (2000).
[26] W. Urban, A. Zlomaniec, G. S. Simpson, H. Faust, T. Rzaca-Urban, and M. Jentschel, Phys. Rev. C **79**, 037304 (2009).
[27] P. Bhattacharyya, P. J. Daly, C. T. Zhang, Z. W. Grabowski, S. K. Saha, B. Fornal, R. Broda, W. Urban, I. Ahmad, D. Seweryniak *et al.*, Phys. Rev. C **64**, 054312 (2001).
[28] P. Datta, S. Chattopadhyay, P. Banerjee, S. Bhattacharya, B. Dasmahapatra, T. K. Ghosh, A. Goswami, S. Pal, M. S. Sarkar, S. Sen *et al.*, Phys. Rev. C **69**, 044317 (2004).
[29] P. Joshi, M. P. Carpenter, D. B. Fossan, T. Koike, E. S. Paul, G. Rainovski, K. Starosta, C. Vaman, and R. Wadsworth, Phys. Rev. Lett. **98**, 102501 (2007).
[30] E. O. Lieder, R. M. Lieder, R. A. Bark, Q. B. Chen, S. Q. Zhang, J. Meng, E. A. Lawrie, J. J. Lawrie, S. P. Bvumbi, N. Y. Kheswa *et al.*, Phys. Rev. Lett. **112**, 202502 (2014).
[31] C. Liu, S. Y. Wang, B. Qi, D. P. Sun, S. Wang, C. J. Xu, L. Liu, P. Zhang, Z. Q. Li, B. Wang *et al.*, Phys. Rev. C **88**, 037301 (2013).
[32] S. Roy, N. Rather, P. Datta, S. Chattopadhyay, R. A. Bark, S. Pal, S. Bhattacharya, R. K. Bhowmik, A. Goswami, H. C. Jain *et al.*, Phys. Lett. B **710**, 587 (2012).
[33] X. Hao *et al.*, Chin. Phys. C **32**(S2), 143 (2008).
[34] S. H. Liu, J. H. Hamilton, A. V. Ramayya, Y. S. Chen, Z. C. Gao, S. J. Zhu, L. Gu, E. Y. Yeoh, N. T. Brewer, J. K. Hwang *et al.*, Phys. Rev. C **83**, 064310 (2011).
[35] Y. X. Luo, J. O. Rasmussen, C. S. Nelson, J. H. Hamilton, A. V. Ramayya, J. K. Hwang, S. H. Liu, C. Goodin, N. J. Stone, S. J. Zhu *et al.*, Nucl. Phys. A **874**, 32 (2012).
[36] F. R. Xu, P. M. Walker, and R. Wyss, Phys. Rev. C **65**, 021303(R) (2002).
[37] Y. X. Luo, J. O. Rasmussen, J. H. Hamilton, A. V. Ramayya, S. Frauendorf, J. K. Hwang, N. J. Stone, S. J. Zhu, N. T. Brewer, E. Wang *et al.*, Nucl. Phys. A **919**, 67 (2013).
[38] P. Möller, J. R. Nix, W. D. Myers, and W. J. Swiatecki, At. Data Nucl. Data Tables **59**, 185 (1995).
[39] A. Bhat, A. Bharti, and S. K. Khosa, Eur. Phys. J. A **48**, 39 (2012).
[40] S. H. Liu, J. H. Hamilton, A. V. Ramayya, A. Gelberg, L. Gu, E. Y. Yeoh, S. J. Zhu, N. T. Brewer, J. K. Hwang, Y. X. Luo *et al.*, Phys. Rev. C **84**, 014304 (2011).
[41] W. D. Myers and W. J. Swiatecki, Nucl. Phys. **81**, 1 (1966).
[42] W. Nazarewicz, J. Dudek, R. Bengtsson, T. Bengtsson, and I. Ragnarsson, Nucl. Phys. A **435**, 397 (1985).
[43] H. C. Pradhan, Y. Nogami, and J. Law, Nucl. Phys. A **201**, 357 (1973).
[44] F. R. Xu, P. M. Walker, J. A. Sheikh, and R. Wyss, Phys. Lett. B **435**, 257 (1998).
[45] Y. Sun, D. H. Feng, and S. X. Wen, Phys. Rev. C **50**, 2351 (1994).